Materials Transactions, JIM, Vol. 32, No. 8 (1991), pp. 679 to 688

Mechanism of the Transition from Bainite to Acicular Ferrite

S. S. Babu* and H. K. D. H. Bhadeshia*

The factors controlling the transition from a microstructure consisting of austenite grain boundary nucleated sheaves of bainite, to one containing intragranularly nucleated plates of acicular ferrite are explored. The work confirms that in weld metals containing inclusions, the transition from bainite to acicular ferrite can be stimulated by the prior formation of a small amount of allotriomorphic ferrite along the austenite grain surfaces. For a successful transition, the allotriomorphic ferrite has to be inert, i.e. unable to develop into Widmanstätten ferrite or bainite sheaves. Detailed experiments are reported to verify that the allotriomorphic ferrite can be rendered inert by the build up of carbon in the austenite ahead of the allotriomorphic ferrite/austenite boundary.

(Received March 28, 1991)

Keywords: *bainite, acicular ferrite, welding, mechanism, kinetics, thermodynamics*

I. Introduction

Acicular ferrite is a phase most commonly observed due to the transformation of austenite during the cooling of low-alloy steel arc-weld deposits (see for example, Ref. (1)–(4)). It is also found in wrought steels which have deliberately been inoculated with nonmetallic inclusions[5]-[8]. Acicular ferrite is of considerable commercial importance because it provides a relatively tough and strong microstructure.

A lot of experimental data have provided convincing evidence that acicular ferrite is essentially intragranularly nucleated bainite[3][4][9]-[12]. Acicular ferrite does not normally grow in sheaves because the development of sheaves is stifled by hard impingement between plates nucleated independently at adjacent sites[10]. Indeed, conventional bainite or acicular ferrite can be obtained under identical isothermal transformation conditions in the same (inclusion rich) steel; to obtain bainite, the austenite grain size has to be small in order that nucleation from grain surfaces dominates and subsequent growth then swamps the interiors of the austenite grains[10]. For a larger austenite grain size, intragranular nucleation on inclusions dominates, so that acicular ferrite is obtained. Using the same reasoning, acicular ferrite is not found when the number density of intragranular nucleation sites is small[13]. Some of the experimental results which confirm that acicular ferrite is nothing but intragranularly nucleated bainite are summarised schematically in Fig. 1. The transformation temperatures are identical for all the cases illustrated, the differences being that: (Fig. 1(a)) inclusion density changed for the same austenite grain size — the sample with the smaller inclusion density transforms to bainite since the relative number density of austenite grain boundary nucleation sites is larger[13]; (Fig. 1(b)) an increase in the austenite grain size at constant inclusion density stimulates a transition from a predominantly bainitic to an acicular ferrite microstructure[10]; (Fig. 1(c)) the growth of a layer of inert allotriomorphic ferrite at the austenite grain surfaces causes a transition from bainite to acicular ferrite[12]†.

II. Method and Experimental Techniques

To enable the acicular ferrite/bainite transition to be studied easily, it is necessary that the steel used should contain a substantial quantity of nonmetallic inclusions of the type responsible for the nucleation of acicular ferrite. Consequently, steel samples were machined from a manual metal arc weld, deposited in a way designed to avoid significant dilution from the base material (i.e. an all weld metal deposit to ISO 2560 joint geometry). The weld was deposited using 4 mm diameter electrodes, 120 Amps current, 23 V DC+ potential, 250°C interpass temperature and 4 mm s^{-1} welding speed. The joint was deposited on 20 mm thick mild steel base plate, with some 30 runs necessary to complete the weld. The final chemical composition is given in Table 1, determined

Table 1 Chemical composition (mass%) of the alloy used in this investigation. The nitrogen and oxygen concentrations are in parts per million by mass.

C	Si	Mn	Ni	Mo	Cr	Al	Ti	O	N
0.10	0.68	1.24	0.04	0.01	1.87	0.007	0.015	274	168

* University of Cambridge/JRDC, Department of Materials Science & Metallurgy, Pembroke St., Cambridge CB2 3QZ, U.K.

† Henceforth, *active* allotriomorphic ferrite is defined as that which is able to develop into other transformation products such as Widmanstätten ferrite or bainite at the transformation temperature of interest. The allotriomorphic ferrite is said to be *inert* when the local reduction in transformation temperature at the ferrite/austenite interface due to the partitioning of carbon prevents the development of secondary Widmanstätten ferrite or bainite.

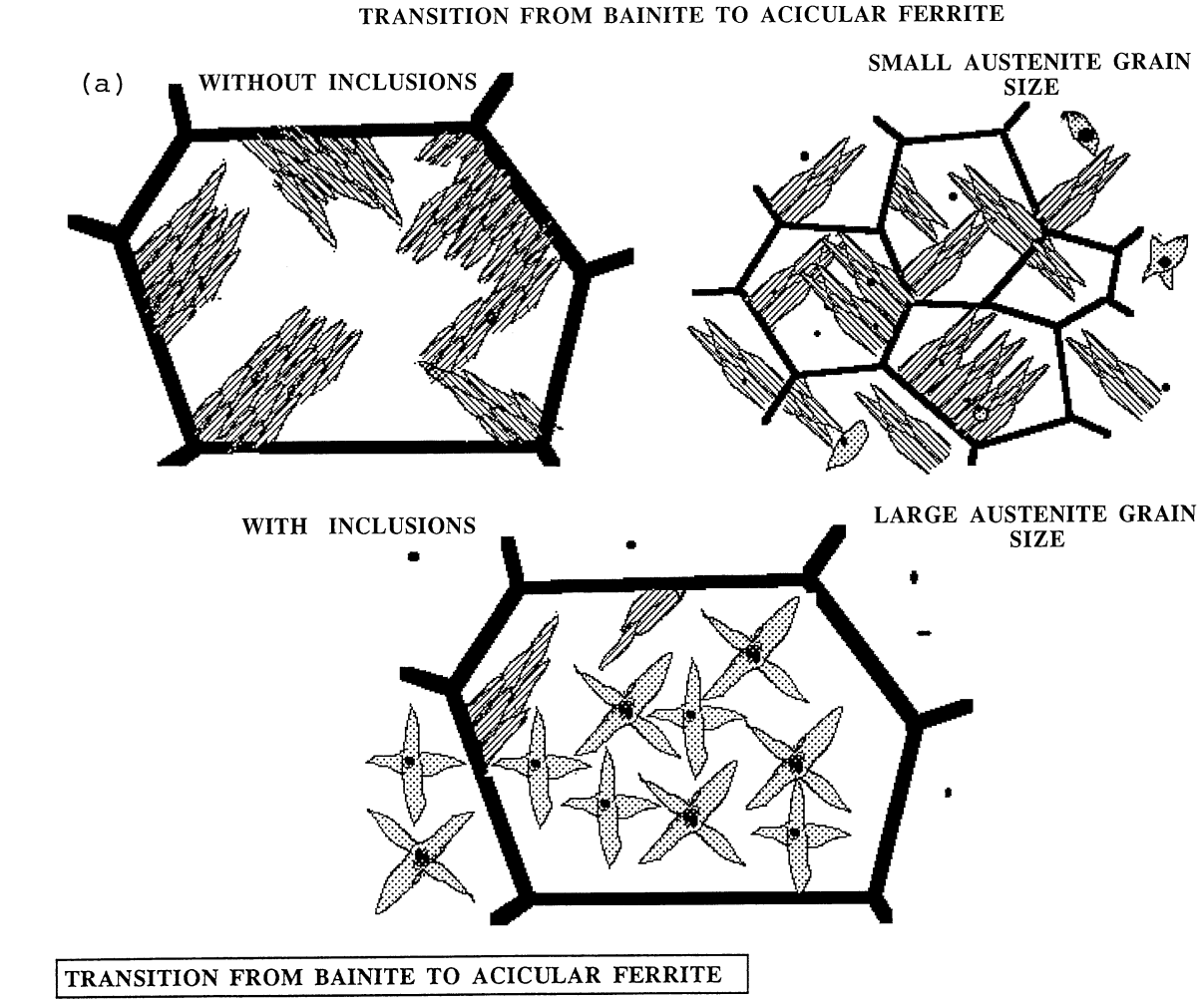

Fig. 1 Schematic illustration of some of the experiments which indicate that acicular ferrite is nothing but intragranularly nucleated bainite. The transformation temperatures are identical for all samples, the differences being that: (a) inclusion density changed for the same austenite grain size—the sample with the smaller inclusion density transforms to bainite since the relative number density of austenite grain boundary nucleation sites is larger[13]; (b) an increase in the austenite grain size at constant inclusion density stimulates a transition from a predominantly bainitic to an acicular ferrite microstructure. (c) The growth of a layer of inert allotriomorphic ferrite at the austenite grain surfaces causes a transition from bainite to acicular ferrite.

spectroscopically with the oxygen and nitrogen concentrations being measured using LECO furnaces.

The samples machined from the weld, in the form of 3 mm diameter rods, were homogenised at 1200°C for 3 days, while sealed in quartz tubes containing pure argon. The samples were then plated with a thin layer of nickel, as described elsewhere[10], in order to minimise surface effects. All subsequent heat-treatments were conducted in a *Theta Industries* high-speed dilatometer with a helium gas-quench facility. The austenitisation treatment was carried out under helium in the dilatometer chamber.

For optical microscopy, the samples were mechanically polished and etched in 2% nital solution. The prior austenite grain size generated by austenitising at 1150°C for 10 min was found to be about 70 μm (mean lineal intercept).

Thin foils for transmission electron microscopy were prepared from 0.3 mm thick discs cut from the heat-treated rods. The discs were mechanically thinned to about 70 μm by abrasion on SiC coated grinding paper, and then electropolished in a solution of 5% perchloric acid, 25% glycerol and 70% ethyl alcohol, at a potential of 65 V (5°C). The thin foil samples were examined using a *Philips EM-400T* transmission electron microscope operated at 120 kV.

Details of the dilatometric technique have been described previously[12]; the interpretation of such data requires a knowledge of lattice parameters and thermal expansivities of the phases involved. The lattice parameter of ferrite was measured using X-ray diffraction (Debye-Scherrer, Cu-K_α, 45 kV). With a Nelson-Riley extrapolation of the measured data, the accurate ferrite lattice parameter was found to be 0.28739 ± 0.00024 nm. For austenite, the lattice parameter can be estimated using published data[14][15]. The thermal expansion coefficients of austenite and ferrite were measured dilatometrically to be $1.9955 \times 10^{-5} \pm 0.2 \times 10^{-7}\ K^{-1}$ and $1.3941 \times 10^{-5} \pm 0.2 \times 10^{-7}\ K^{-1}$ respectively.

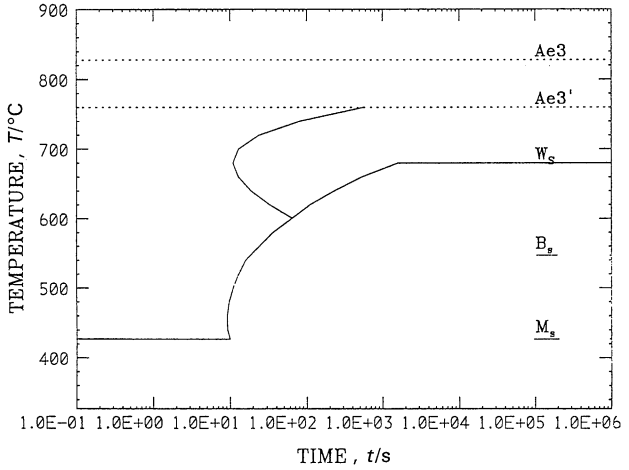

Fig. 2 Calculated time-temperature-transformation diagram for the alloy studied. The thermodynamically calculated transformation temperatures (°C) are $M_S = 427$, $B_S = 546$, $W_S = 680$, $Ae_3' = 760$ and $Ae_3 = 828$ representing the martensite-start, bainite-start, Widmanstätten ferrite-start, paraequilibrium $\gamma/(\gamma+\alpha)$ temperature and equilibrium $\gamma/(\gamma+\alpha)$ temperature respectively. Paraequilibrium means that the ferrite grows in such a way that the substitutional solute to iron atom ratio is constant everywhere, whereas equilibrium allows all the alloying elements to partition between the phases.

III. Results and Discussion

1. Heat-treatment

Figure 2 illustrates the calculated[16]-[19] time-temperature-transformation (TTT) diagram for the alloy. If thin layers of allotriomorphic ferrite (α) are to be utilised in order to prevent austenite (γ) grain boundary nucleated reactions from stifling the development of intragranularly nucleated acicular ferrite, then the allotriomorphic ferrite itself must be inert. It is well known, however, that Widmanstätten ferrite packets or bainite sheaves are often seen to grow from α/γ interfaces, especially[20] when the α has an orientation with the austenite which is in the Bain region[21]. In other circumstances, the ferrite appears unable to develop into other transformation products[12]. A major purpose of this work was to investigate whether it is the carbon diffusion field established at a temperature T_α in front of the allotriomorphic ferrite/austenite interface that sometimes prevents the ferrite from developing into Widmanstätten ferrite or bainite during subsequent transformation at a lower temperature T_b.

A series of experiments was designed to investigate the role of the partitioned carbon (Fig. 3, Table 2); the detailed choice of transformation temperatures for these experiments is discussed later:

(a) Heat-treatment H1 involved a low allotriomorphic ferrite transformation temperature (T_α), in order to render it inert (a low T_α corresponds to a large value of $x^{\gamma\alpha}$, the carbon concentration in the austenite at the austenite/ferrite interface).

(b) As a control experiment, H2 was designed with a high T_α, such that the allotriomorphic ferrite would be active on subsequent transformation at T_b.

(c) Any carbon build up at the α/γ interface can in principle be homogenised by annealing at a high temperature $T_a > T_\alpha$. This could render initially inert allotriomorphic ferrite active. Heat-treatments H3 and H4 were designed to test this idea.

(d) In heat-treatment H5, the temperature T_b was deliberately set to be larger than the bainite-start temperature of the alloy, in order to confirm that acicular ferrite, which is supposed to be intragranularly nucleated bainite, does not form.

The temperatures for the heat-treatments just described were determined theoretically, by calculating the Widmanstätten ferrite-start and bainite-start temperatures for the austenite (of composition $x^{\gamma\alpha}$) adjacent to the allotriomorphic ferrite, as illustrated in Fig. 4. In Fig. 4, the horizontal axis represents the temperature at which allotriomorphic ferrite grows, whereas the vertical axis represents the Widmanstätten ferrite-start or bainite-

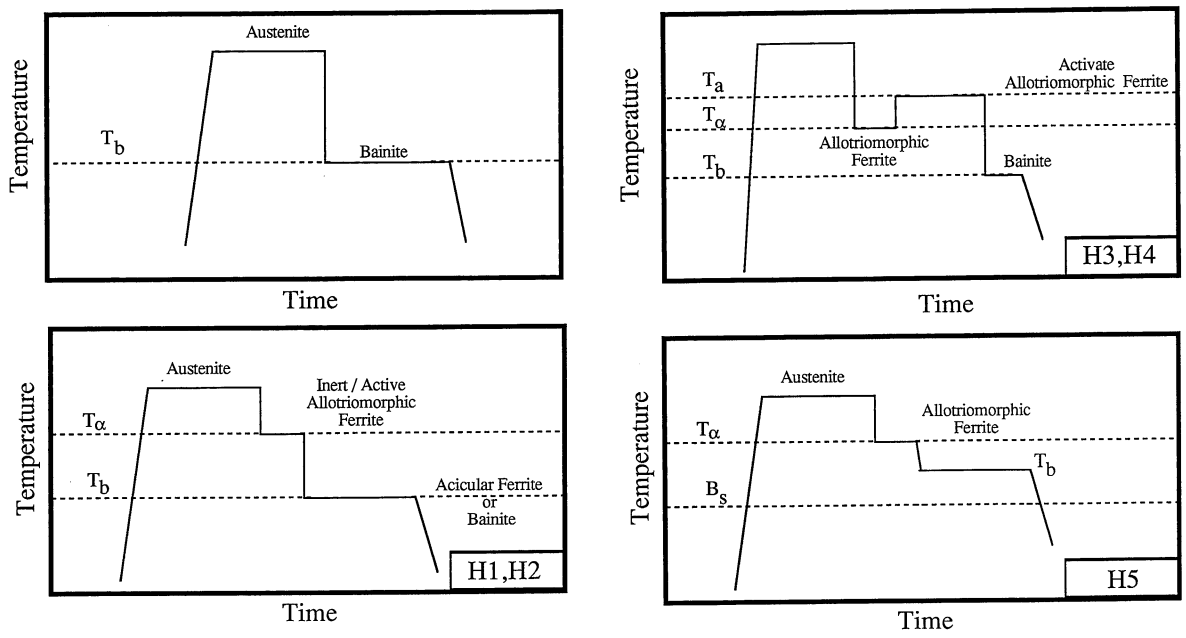

Fig. 3 Schematic illustration of the heat-treatments used.

Table 2 Heat-treatment schedules. The samples were austenitised at 1150°C for 10 min prior to transformation at lower temperatures. The temperatures (T) are all stated in °C, and the corresponding time periods (t) in minutes. The samples were all quenched after the final isothermal reaction. T_α is the allotriomorphic ferrite growth temperature, T_a is an annealing temperature and T_b is a bainitic transformation temperature.

	T_α	t_α	T_a	t_a	T_b	t_b
H1	660	1.0	—	—	501	5
H2	740	4.0	—	—	500	60
H3	660	1.0	760	0.5	500	60
H4	660	1.0	750	1.0	500	60
H5	660	1.0	—	—	600	1

start temperature of the austenite at the allotriomorphic ferrite/austenite interface. The methods for thermodynamic and transformation-start calculations have been described elsewhere[16]-[19]. It is clear from Fig. 4 that for $T_\alpha=660$°C, the allotriomorphic ferrite is expected to be inert when $T_b=500$°C. For the same value of $T_b=500$°C, allotriomorphic ferrite generated by transformation at $T_\alpha>720$°C is expected to be active.

These calculations are valid for heat-treatments H1 and H2, which do not include any intermediate annealing treatment at T_a. They assume therefore that any carbon concentration built up in the austenite as the allotriomorph grows, is retained as the sample is cooled rapidly to T_b. On the other hand, samples H3 & H4 were annealed at T_a immediately after the growth of allotriomorphic ferrite and before heat-treatment at T_b. It is therefore necessary to model any change in the carbon concentration profile ahead of the α/γ interface during the annealing treatment.

The distribution of carbon (x) in front of a ferrite

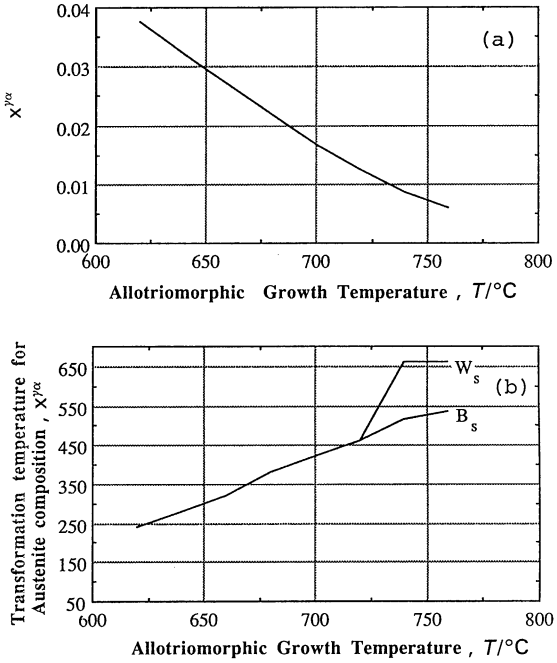

Fig. 4 Calculations designed to predict whether the allotriomorphic ferrite should be inert or active. (a) Variation of $x^{\gamma\alpha}$ as a function of the temperature at which allotriomorphic ferrite grows. (b) The horizontal axis represents the temperature at which allotriomorphic ferrite is induced to form. The vertical axis represents the Widmanstätten ferrite-start or bainite-start temperature of the austenite at the allotriomorphic ferrite/austenite interface.

allotriomorph of half-thickness Z in the absence of soft-impingement is given by[22][23]

$$x\{z,t\}=\bar{x}+(x^{\gamma\alpha}-\bar{x})\left[\frac{1-\mathrm{erf}\{z/(4\underline{D}t)^{0.5}\}}{1-\mathrm{erf}\{Z/(4\underline{D}t)^{0.5}\}}\right] \quad (1)$$

where z is the distance in the austenite ahead of the interface, and $\bar{x}$ is the average carbon concentration of the

steel. $\underline{D}$ is the weighted average carbon diffusivity in austenite[24]:

$$\underline{D}=\int_{x^{\gamma\alpha}}^{\bar{x}} D\{x\}\,\mathrm{d}x/(\bar{x}-x^{\gamma\alpha}) \qquad (2)$$

where D is the concentration dependent diffusion coefficient of carbon in austenite, calculated as in (25)–(27).

Having calculated this carbon concentration profile generated at T_α, a finite difference method described elsewhere[12] was utilised to see how it homogenises during heat-treatment at T_a (Fig. 5). The concentration at the ferrite/austenite boundary after the annealing treatment is therefore known, permitting the calculation of Widmanstätten ferrite-start and bainite-start temperatures at that location. With the help of such calculations, it was possible to demonstrate (Table 3) that heat-treatments H3 and H4, both of which incorporate an intermediate anneal at T_a, should activate the ferrite which would otherwise be inert. The ferrite half-thickness values necessary for the calculations were measured directly using optical microscopy at about 3.5 μm. This probably overestimates the thickness due to sectioning errors. The calculations nevertheless demonstrated that even with any overestimated thickness, the annealing treatment is more than adequate in activating the ferrite.

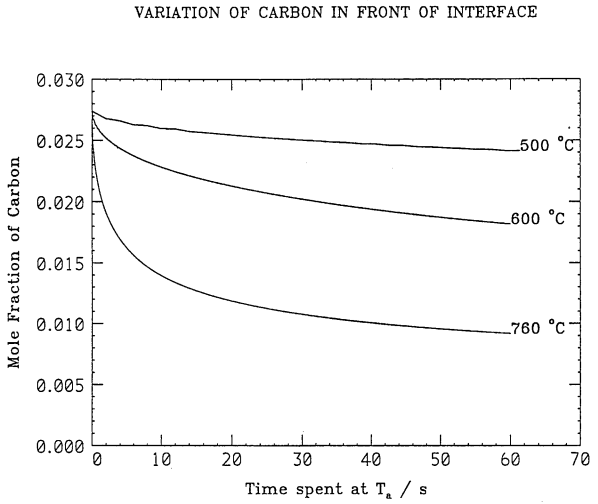

Fig. 5 Finite-difference modelling of the homogenisation of the carbon concentration profile generated during the growth of allotriomorphic ferrite. The figure shows variation of $x^{\gamma\alpha}$ as a function of time at a given ageing temperature T_a. Notice that the ageing heat-treatment at 500°C (the temperature at which bainite or acicular ferrite are formed) hardly reduces the $x^{\gamma\alpha}$, in comparison to heat-treatment at 760°C.

Table 3 The results of calculations designed to indicate whether the allotriomorphic ferrite generated in heat-treatments H1–H4 should be inert or active. $x^{\gamma\alpha}_{T_\alpha}$ is the carbon concentration in the austenite at the α/γ interface at the temperature T_α. $x^{\gamma\alpha}_{T_a}$ is the carbon concentration in the austenite at the α/γ after heat-treatment at T_a. Since $T_b=500$°C, $x^{\gamma\alpha}_{T_a}$ must be less than 0.011 mole fraction if the ferrite is to be active during isothermal holding at T_b. The microstructure observed experimentally (within the austenite grains) is listed in the last column. The concentrations are all in mole fractions, the temperatures in °C and time in minutes.

	T_α	t_α	$x^{\gamma\alpha}_{T_\alpha}$	T_a	t_a	$x^{\gamma\alpha}_{T_a}$	Microstructure
H1	660	1.0	0.0274	501	5	0.0224	acicular
H2	740	4.0	0.0086	500	60	0.0079	bainite
H3	660	1.0	0.0274	760	0.5	0.0119	bainite
H4	660	1.0	0.0274	750	1.0	0.0092	bainite

Figure 6 shows the microstructure of a sample which was quenched directly from the austenitisation temperature to another temperature (500°C) below B_S. The experiment confirms that in ordinary circumstances, heterogeneous nucleation at the austenite grain surfaces dominates the transformation behaviour, leading to a fully bainitic microstructure rather than one containing intragranularly nucleated bainite (i.e. acicular ferrite). This is in complete contrast with the microstructure obtained during heat-treatment H1 (Fig. 7), in which the first transformation product to form is allotriomorphic ferrite, which completely decorates the austenite grain surfaces. Since this allotriomorphic ferrite is inert (Table 3), transformation at T_b leads to the formation of acicular ferrite.

Figure 8 (heat-treatment H2) shows a case where the allotriomorphic ferrite is ineffective. Because it formed at a relatively higher temperature, $x^{\gamma\alpha}_{T_\alpha}$ is small enough to permit the ferrite to develop into bainite during transformation at T_b. There is clear evidence of the growth of bainite sheaves from the allotriomorphic ferrite (which is therefore classified to be active, Table 3); consistent with theory, bainite is obtained instead of acicular ferrite.

Fig. 6 The bainitic microstructure generated during isothermal transformation at 500°C for 60 min followed by quenching to ambient temperature.

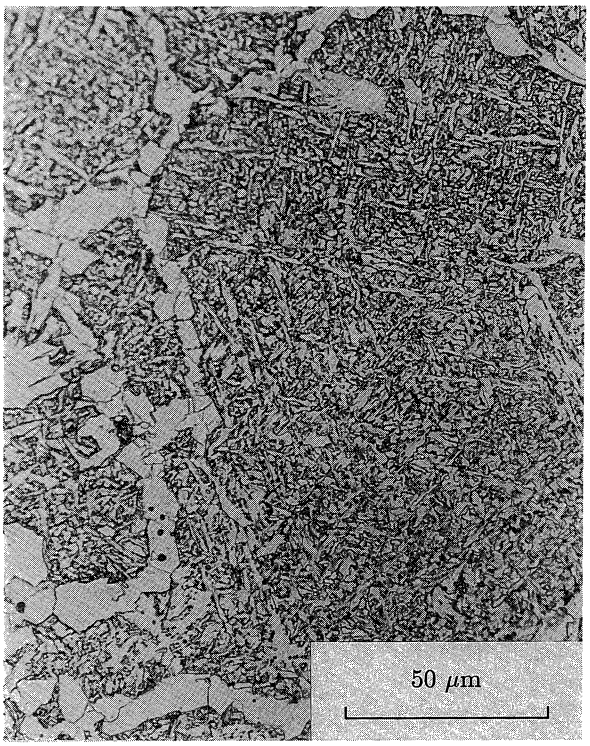

Fig. 7 The microstructure generated by heat-treatment H1. The allotriomorphic ferrite layer is inert, giving acicular ferrite in the interiors of the austenite grains.

Experiments H3 and H4 both show bainitic microstructures (Fig. 9(a) and (b)), because in both cases, the annealing treatment at T_a leads to a reduction in the concentration of carbon at the α/γ interface, rendering the allotriomorphic ferrite active.

Figure 10 confirms that acicular ferrite will not form if T_b is greater than the bainite-start temperature of the alloy, even when the austenite grain boundaries are covered with layers of inert allotriomorphic ferrite. Heat-treatment H5 has a microstructure of just allotriomorphic ferrite and the martensite obtained on quenching to ambient temperature.

2. Interpretation of dilatometric data

The dilatometric technique can be extremely useful in studying transformations because it allows the transformation to be followed as it happens (Fig. 11). The three typical examples presented in Fig. 11 illustrate direct transformation to bainite, a two-stage heat-treatment involving first the formation of allotriomorphic ferrite

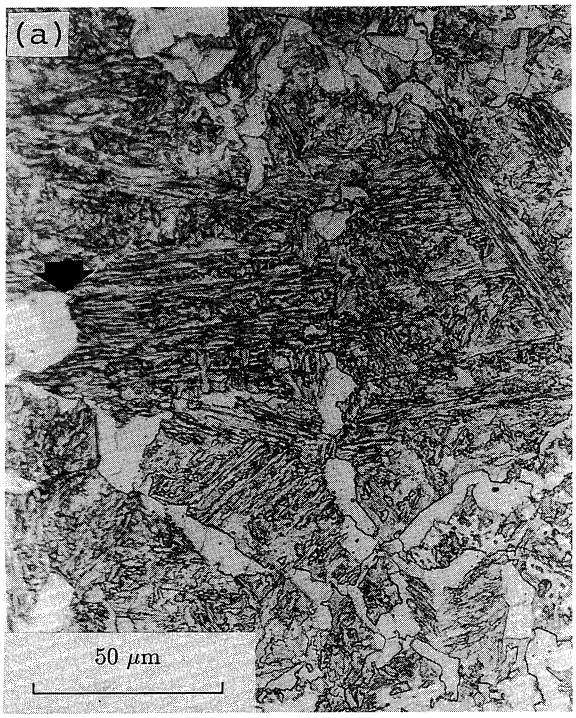

Fig. 8 The microstructure generated by heat-treatment H2, in which the allotriomorphic ferrite is active, with bainite sheaves in the middle of the austenite grains, (a) optical micrograph, (b) thin foil transmission electron micrograph of allotriomorphic ferrite and bainite sheaf.

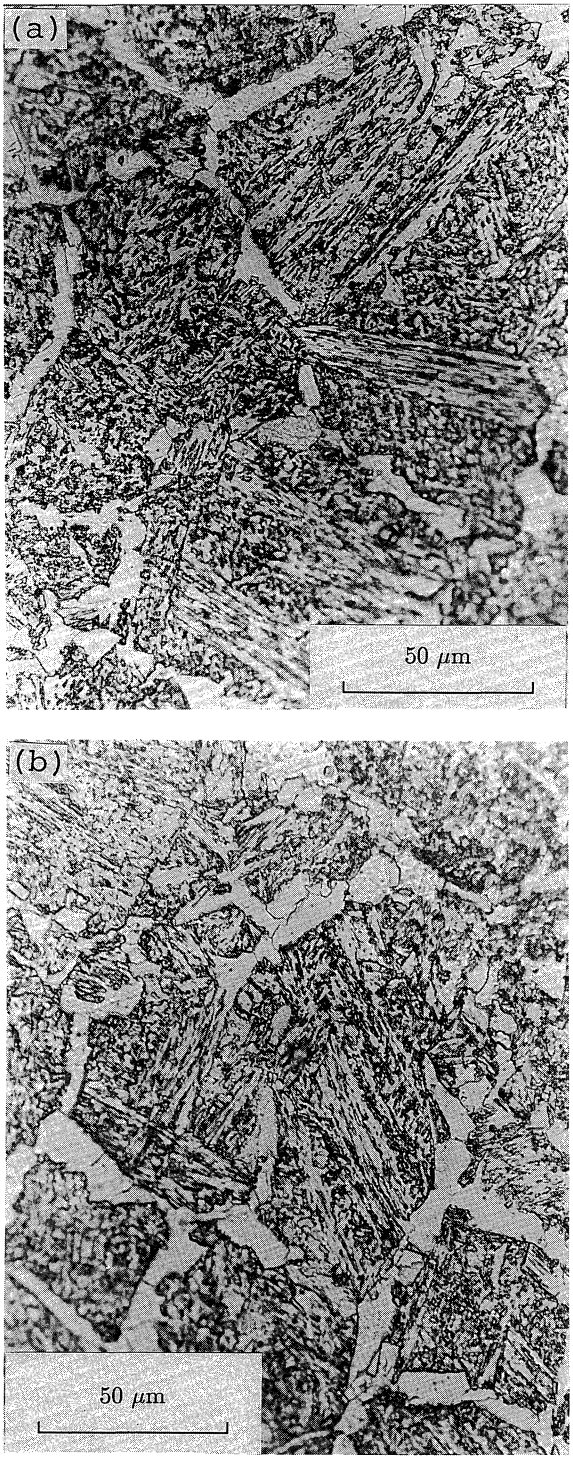

Fig. 9 The microstructures generated by heat-treatments H3 (a) and H4 (b), where the allotriomorphic ferrite was activated by annealing at 760 and 750°C, respectively. Bainite sheaves have formed as a consequence.

and then acicular ferrite, and finally, a three-stage heat-treatment in which the sample is annealed at an elevated temperature after the growth of allotriomorphic ferrite. It is particularly notable that in the latter case, no transformation occurs during annealing at T_a, although the distribution of carbon must homogenise as discussed earlier. This is because the paraequilibrium fraction of

Fig. 10 The microstructure generated by heat-treatment H5, consisting of allotriomorphic ferrite and martensite, since isothermal holding at a temperature above B_S did not cause any transformation.

ferrite at T_a is approximately that which was induced to form at T_α.

Figure 12(a) illustrates the length change observed during isothermal transformation at 660°C; the incubation time prior to the onset of substantial reaction is about 10 s, which is consistent with the calculated TTT diagram presented in Fig. 2. Figure 12(b) shows how the isothermal transformation at temperatures below B_S (500°C) ceases, (B_S temperature, for average composition determined using the method presented elsewhere[16)-(19)], is 546°C) so that the carbon concentration of the residual austenite at that stage can be compared against the T_0' curve (discussed later) in order to deduce the mechanism of transformation.

The dilatometric data can be interpreted further, since the length changes can be converted into the volume fraction of transformation using the lattice parameter and thermal expansivity measurements presented earlier[15]. The volume fraction data can in turn be combined with a conservation of mass criterion to estimate the carbon concentration of the residual austenite at any stage of reaction. It is interesting to see that for heat-treatments H1 and H4, the formation of acicular ferrite and bainite (respectively) ceases as the carbon concentration of the residual austenite reaches the T_0' curve of the phase diagram (Fig. 13). This curve defines the locus of all points on the phase diagram at which austenite and strained-ferrite of the same composition have the same free energy (see for example, (4)). If that carbon concentration is exceeded, then transformation cannot proceed

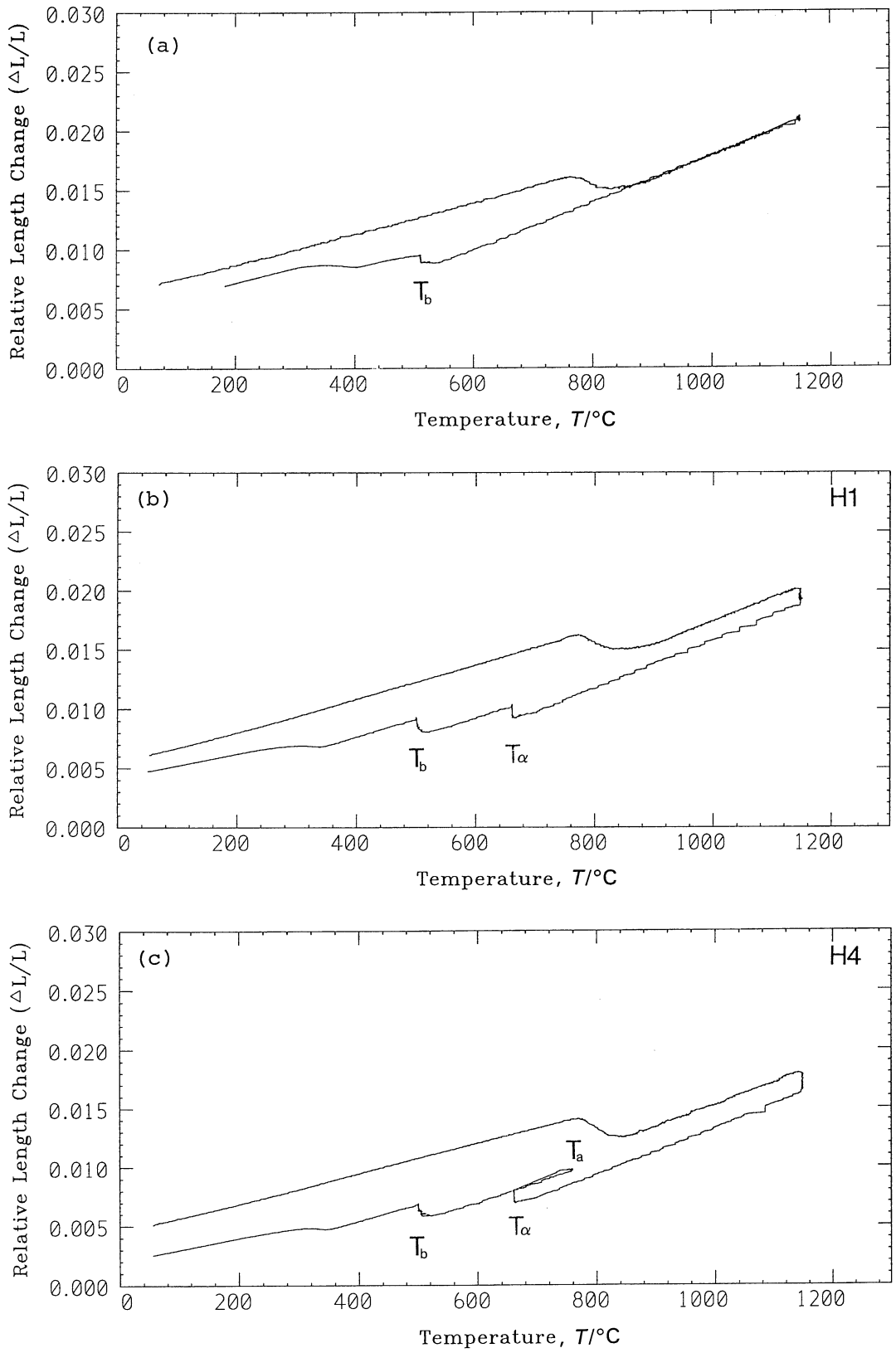

Fig. 11 Dilatometric data: (a) direct transformation below the bainite-start temperature; (b) two-stage heat-treatment in which the initial transformation to allotriomorphic ferrite is followed by further transformation below B_S; (c) as in (b), but with an elevated temperature anneal imposed between the allotriomorphic and bainitic transformation to homogenise carbon in the residual austenite.

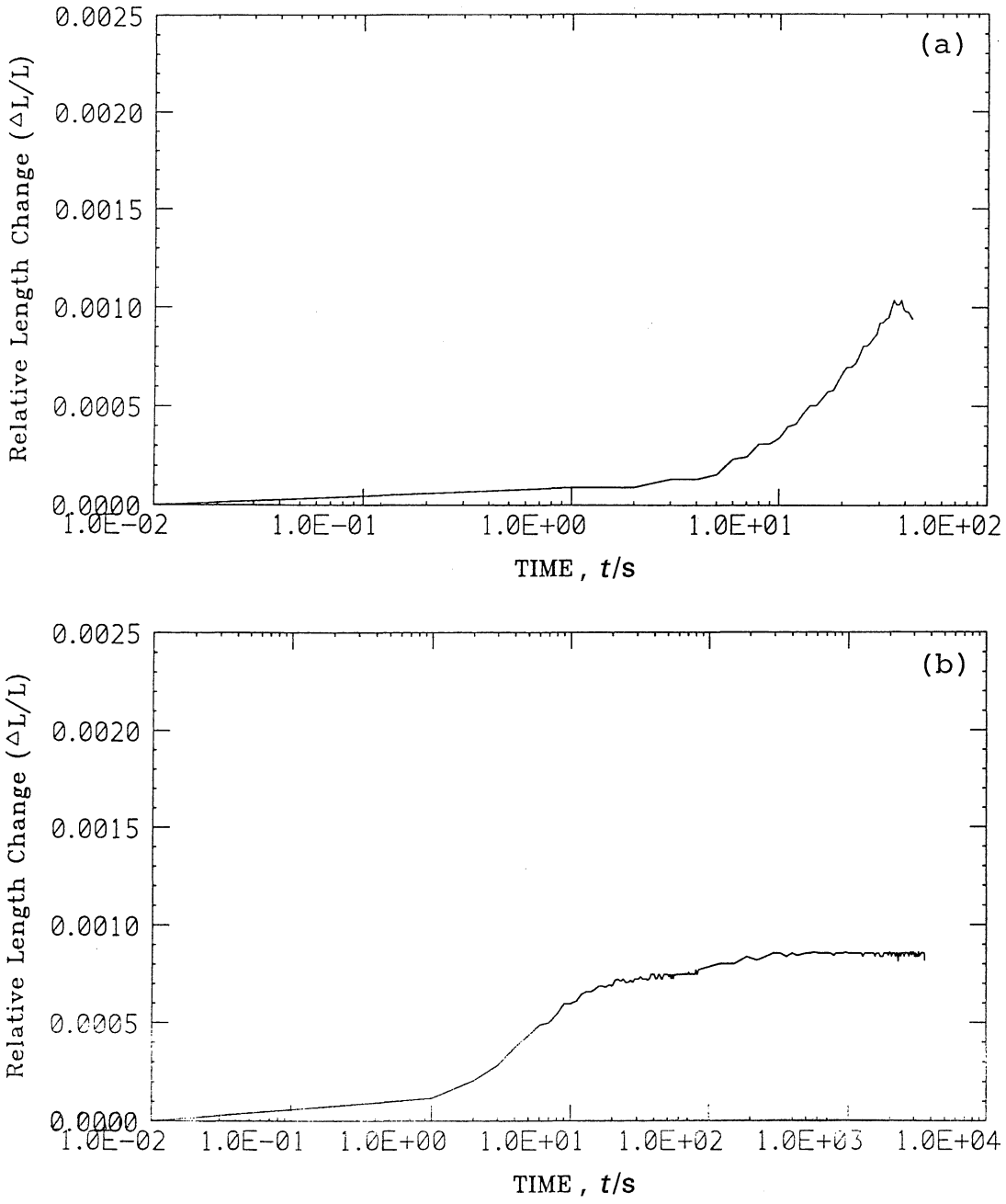

Fig. 12 (a) Dilatometric data showing that substantial transformation begins after about 10 s at 660°C, consistent with the calculated TTT diagram of Fig. 2. (b) Illustration of the fact that isothermal transformation at 500°C within the bainite transformation temperature range leads to a fairly rapid cessation of reaction, permitting the carbon concentration of residual austenite at that stage to be compared against the T_0' phase boundary.

without the partitioning of carbon. Bainite[4] and acicular ferrite[9][10] are both known to stop growing when the T_0' curve is reached, indicating the existence of an *incomplete reaction phenomenon* which can be interpreted to indicate that bainite and acicular ferrite grow without diffusion, any partitioning of carbon occurring after the growth event. These results are therefore significant in two respects; firstly, acicular ferrite is once again confirmed to have the same mechanism of transformation as bainite. The second point is that the enrichment of austenite caused by the initial partial transformation to allotriomorphic ferrite also contributes to an early cessation of transformation to bainite or acicular ferrite.

IV. Conclusions

The formation of acicular ferrite in steels containing intragranular nucleation sites can be enhanced by reducing the number density of austenite grain boundary nucleation sites. This can be done by decorating the austenite grain surfaces with thin layers allotriomorphic ferrite. The ferrite must however, be inert in the sense that it

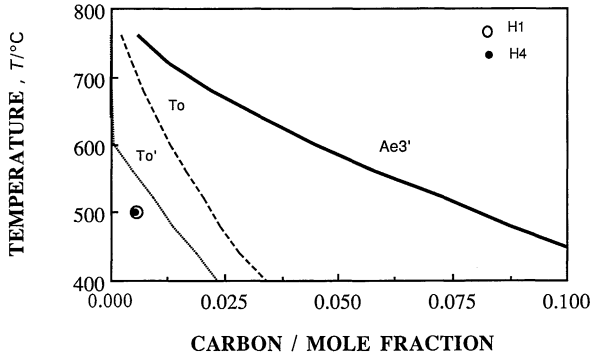

Fig. 13 The carbon concentrations of the austenite that is left untransformed after the cessation of the acicular ferrite or bainitic transformation (in a mixed microstructure which also contains some allotriomorphic ferrite), plotted together with calculated phase boundaries. The transformations clearly cease well before the austenite reaches its paraequilibrium or equilibrium composition.

should not develop at lower transformation temperatures into secondary Widmanstätten ferrite or bainite. It can be rendered inert by the partitioning of carbon into the austenite at the ferrite/austenite interface, as long as the local concentration is large enough to depress the local Widmanstätten ferrite-start or bainite-start temperature below the actual heat-treatment temperature. Finally, the results are all consistent with the hypothesis that acicular ferrite is nothing but intragranularly nucleated bainite.

Acknowledgements

We are grateful to Professor C. J. Humphreys (University of Cambridge) for the provision of laboratory facilities. Thanks are also due to Dr. Lars-Erik Svensson (ESAB AB) for providing the welds. One of the authors (SSB) also wishes to thank the Cambridge Commonwealth Trust for providing the financial aid for this study and also the Council of Vice Chancellors and Principals of the United Kingdom for an overseas research students award. HKDHB's contribution to this work was carried out under the auspices of the "Atomic Arrangements: Design and Control" project, which is a collaborative venture between the Research and Development Corporation of Japan and the University of Cambridge.

REFERENCES

(1) O. Grong and D. K. Matlock: International Metals Reviews, **31** (1986), 27.
(2) D. J. Abson and R. J. Pargeter: International Metals Reviews, **31** (1986), 141.
(3) H. K. D. H. Bhadeshia: *Recent Trends in Welding Science and Technology TWR'89*, ed. by S. A. David and J. M. Vitek, ASM International, Ohio, (1989), p. 189.
(4) H. K. D. H. Bhadeshia and J. W. Christian: Metall. Trans. A, **21A** (1990), 767.
(5) M. Imagumbai, R. Chijiiwa, N. Aikawa, M. Nagumo, H. Homma, S. Matsuda and H. Mimura: *HSLA Steels: Metallurgy and Applications*, ed. by J. M. Gray, T. Ko, Z. Shouhua, W. Baorong and X. Xishan, ASM International, Ohio, (1985), p. 557.
(6) K. Yamamoto, S. Matsuda, T. Haze, R. Chijiiwa and H. Mimura: *Residual and Unspecified Elements in Steel*, ASM International, Ohio, (November 1987), p. 1.
(7) K. Nishioka and H. Tamehiro: *Microalloying '88 : International Symposium on Applications of HSLA Steel*, Chicago, Illinois, (September 1988), p. 1.
(8) H. K. D. H. Bhadeshia: *Steel Technology International*, ed. by P. H. Scholes, Sterling Publications International Ltd., London, (1989), p. 289.
(9) M. Strangwood and H. K. D. H. Bhadeshia: *Advances in the Science and Technology of Welding*, ed. by S. A. David, ASM International, Ohio, (1987), p. 209.
(10) J. R. Yang and H. K. D. H. Bhadeshia: *Advances in the Science and Technology of Welding*, ed. by S. A. David, ASM International, Ohio, (1987), p. 187.
(11) A. A. B. Sugden and H. K. D. H. Bhadeshia: Metall. Trans. A, **20A** (1989), 1811.
(12) S. S. Babu and H. K. D. H. Bhadeshia: Mater. Sci. Tech., **6** (1990), 1005.
(13) P. L. Harrison and R. A. Farrar: J. Mater. Sci., **16** (1981), 2218.
(14) D. J. Dyson and B. Holmes: J. Iron Steel Inst., **277** (1970), 469.
(15) H. K. D. H. Bhadeshia: Journal de Physique, **43-C4** (1982), 435.
(16) H. K. D. H. Bhadeshia: Acta Metall., **29** (1981), 1117.
(17) H. K. D. H. Bhadeshia: Metal Sci., **16** (1982), 159.
(18) H. K. D. H. Bhadeshia: Metal Sci., **15** (1981), 175.
(19) H. K. D. H. Bhadeshia: Metal Sci., **15** (1981), 178.
(20) S. S. Babu and H. K. D. H. Bhadeshia: Mater. Sci. Engineering A, (1991), in press.
(21) A. Crosky, P. G. McDougall and J. S. Bowles: Acta Metall., **28** (1980), 1495.
(22) D. E. Coates: Metall. Trans., **14** (1973), 395.
(23) H. K. D. H. Bhadeshia: Progress in Mater. Sci., **29** (1985), 321.
(24) R. Trivedi and G. M. Pound: J. Appl. Phys. **38** (1967), 3569.
(25) R. H. Siller and R. B. McLellan: Metall. Trans. A, **1** (1970), 985.
(26) R. H. Siller and R. B. McLellan: Trans. Met. Soc. AIME, **245** (1969), 697.
(27) H. K. D. H. Bhadeshia: Metal Sci., **15** (1981), 477.